Imaging the Subcellular Structure of Human Coronary Atherosclerosis Using 1-μm Resolution Optical Coherence Tomography (μOCT)

Linbo Liu[1,2], **Joseph A. Gardecki**[1,2], **Seemantini K. Nadkarni**[1,2,4], **Jimmy D. Toussaint**[1,2], **Yukako Yagi**[1,3], **Brett E. Bouma**[1,2,4], and **Guillermo J. Tearney**[1,3,4]

[1] Harvard Medical School, Wellman Center for Photomedicine, Massachusetts General Hospital, 50 Blossom Street BAR7, Boston, Massachusetts 02114, USA

[2] Department of Dermatology, Massachusetts General Hospital, Fruit Street, Boston, Massachusetts 02114, USA

[3] Department of Pathology, Massachusetts General Hospital, Fruit Street, Boston, Massachusetts 02114, USA

[4] Harvard-MIT Health Sciences and Technology, Cambridge, MA 02138, USA

Abstract

Progress in understanding, diagnosis, and treatment of coronary artery disease (CAD) has been hindered by our inability to observe cells and extracellular components associated with human coronary atherosclerosis *in situ*. The current standards for microstructural investigation, histology and electron microscopy, are destructive and prone to artifacts. The highest resolution intracoronary imaging modality, optical coherence tomography (OCT), has a resolution of ~10μm, which is too coarse for visualizing most cells. Here we report a new form of OCT, termed μOCT that has an order of magnitude improved resolution. We show that μOCT images of cadaver coronary arteries provide clear pictures of cellular and subcellular features associated with atherogenesis, thrombosis, and response to interventional therapy. These results suggest that μOCT can complement existing diagnostic techniques for investigating atherosclerotic specimens today and may in the future become a useful tool for cellular and subcellular characterization of the human coronary wall *in vivo*.

CAD and one of its more serious clinical manifestations, acute myocardial infarction (AMI), is a major cause of mortality worldwide. Because of the impact of this disease, topics

relevant to the pathophysiology of CAD, such as the development and progression of coronary atherosclerotic lesions, plaque rupture and coronary thrombosis, and the arterial response to coronary device and pharmacologic therapies are of great importance in medicine. These biological processes, mediated by cells and extracellular components, including endothelium, leukocytes, macrophages, smooth muscle cells, platelets, and fibrin, occur on a microscopic scale. The development of tools for visualizing coronary artery microstructure at the subcellular level in intact human tissue, and ideally within living patients, could therefore open up new opportunities for the study, diagnosis, and treatment of CAD.

Unfortunately, methods for visualizing human coronary atherosclerosis at the subcellular level are limited. Much of our understanding of CAD is based on histologic analysis of stained thin sections from autopsy specimens,[1–4] which provide a static snapshot of the coronary artery's morphology after the patient has died. As histology is subject to artifact, it provides information that is not wholly representative of the tissue in its native state. Furthermore, hundreds of histopathology slides may be required to find specific cellular features because a single slide samples a very small portion of the specimen. Electron microscopy, including scanning electron microscopy (SEM) and transmission electron microscopy (TEM), used to evaluate the luminal surface and thin sections of the artery wall, respectively, has similar limitations.[5–7]

We have even fewer tools for investigating cellular-level microstructure of CAD in patients. The highest resolution coronary imaging modality is intravascular OCT, a catheter-based technique that provides depth-resolved, cross-sectional images of tissue reflectance. With an axial (depth) resolution of approximately 10 μm and a lateral resolution of 30–40 μm,[8–11] intracoronary OCT is capable of characterizing the architectural morphology of plaque at resolution that is 10 times better than intravascular ultrasound (IVUS), the preceding technology for high-resolution imaging of the coronary wall. Current 10-μm resolution intracoronary OCT technology is incapable of identifying individual cells or subcellular structures.

In order to visualize tissue at the cellular level, researchers have continued to push the resolution limits of cross-sectional OCT imaging systems[12–18] in an attempt to achieve an axial resolution of 1 μm and a lateral resolution of 2 μm in tissue, a class of imaging techniques that we term μOCT. We have recently constructed a μOCT system that utilizes a very broad bandwidth light source and common-path[19] spectral-domain OCT (SD-OCT)[20] technology to provide 1-μm-axial resolution ranging in tissue (Supplementary Fig. 1). An annularly apodized,[15] objective lens focuses light within the tissue (Supplementary Fig. 1), providing a lateral resolution of 2 μm. Apodization and chromatic dispersion allow this lateral resolution to be maintained over an extended focal depth.

These technical advances enable cross-sectional imaging of human tissue with axial and lateral resolutions that are approximately an order of magnitude better than conventional OCT systems and devices. This order of magnitude resolution improvement of μOCT may make it possible to image coronary artery microstructure at a scale that is comparable to histopathology (Fig. 1). In this paper, we present μOCT images of human coronary plaques,

which demonstrate the potential of this technology for future study and diagnosis of this prevalent disease.

RESULTS

Our μOCT system obtains images at a rate of 8 frames per second with a resolution of 2 μm × 2 μm × 1 μm (x, y, z) in tissue. We used the μOCT system to image fresh human coronary arteries prosected from explant (donor) hearts. Additional μOCT data was acquired from endothelial cell cultures as well as swine coronary arteries prepared to preserve endothelial morphology. All μOCT images in this paper were acquired in three-dimensions from the luminal surface.

Endothelial cells

Endothelial cells are the gatekeepers for passage of low-density lipoprotein (LDL) and leukocytes into the intima, perform important signalling roles for atherogenesis, plaque progression and regression, and are indicators of arterial healing following stent implantation.[21] In order to demonstrate the capability of μOCT to visualize endothelium, we first imaged cultured cells *in vitro*. A cross-sectional μOCT image of the endothelial cell culture, demonstrated raised structures (arrows) that correspond to cell bodies (Supplementary Fig. 2a). A transverse image of the cultured endothelial cells, derived by reslicing the three-dimensional μOCT image, showed a confluence of stellate-shaped cells (Supplementary Fig. 2b). Two-dimensional μOCT images of swine coronary artery allowed the visualization of endothelial cells *in situ* and also an underlying bright structure that is consistent with an internal elastic lamina (Supplementary Fig. 2c). Three-dimensional volume rendering of the μOCT data showed evidence of endothelial cell "pavementing" (Fig. 2a) that is similar to what one might see by SEM.

Leukocyte adhesion and diapedesis

Leukocyte (T-cell and monocyte) attachment and influx into the intima are key cellular responses that contribute to the formation of atherosclerotic lesions. We discovered that μOCT is capable of visualizing cells likely to be leukocytes adherent to the endothelial surface of human coronary plaques (Figs. 2b–d). μOCT images of presumed leukocyte nuclei demonstrated low image intensity, while the cytoplasm had a comparatively high intensity. This finding suggests that it may be possible to use μOCT to further classify these adherent cells as lymphocytes (small cells with scant cytoplasm), monocytes (larger cells with more abundant cytoplasm and bean-shaped nucleus), and neutrophils (multilobulated nucleus) based on subcellular morphology (Figs. 2b–d). In some μOCT frames, we were also able to visualize processes emanating from these cells, with microstructures reminiscent of pseudopods attaching their bodies to the endothelial surface (Fig. 2e, arrows). Evidence of transmigration was seen by μOCT as an extension of leukocyte cell bodies, presumably monocytes, through the endothelial barrier into the intima (Fig. 2f).

Platelets and fibrin

Thrombus formation, initiated by platelet and fibrin accumulation, is the ultimate pathophysiologic event that leads to coronary artery blockage. Fibrin is also a marker for

inadequate healing over drug-coated stents.[21] Different microscopic clot morphologies could be visualized by μOCT, including arrays of linear structures consistent with fibrin strands (Fig. 2g) and thrombi containing emmeshed cells, presumably leukocytes, and small, highly scattering structures that appear to be platelets with dimensions of 2–3 μm (Fig. 2h).

Macrophages

Once within the intima, monocytes differentiate into macrophages and engulf LDL that has been oxidized by cell byproducts.[22,23] A cycle of cellular signalling and recruitment ensues, resulting in a lesion comprised of collagen, produced by smooth muscle cells, and lipid, which emanates from a variety of sources, including LDL, engorged macrophages (foam cells), and apoptotic macrophages.[24] μOCT images of coronary plaque macrophages appeared as highly scattering, flocculent, round or ellipsoidal cells that are larger than monocytes (Fig. 3a). Spindle-shaped cells with similar high μOCT intensities were also observed in some coronary plaques (Fig. 3b).

Smooth muscle cells

Smooth muscle cells within coronary plaques appeared as spindle-shaped cells by μOCT (Fig. 3c). Two smooth muscle cell microstructural phenotypes were identified in our dataset; the first had a cell body with a low μOCT signal intensity (Fig. 3c, green arrow) and the second had a halo of low μOCT signal surrounding a highly scattering interior (Fig. 3c, red box and inset). Histology showed that smooth muscle cells with a low-intensity halo were producing a collagen matrix (Fig. 3c, inset).

Cholesterol crystals

Cholesterol crystals in atheromatous plaques have recently taken on a greater significance with the suggestion by Abela *et al.* that these crystals may penetrate and weaken fibrous caps, potentially leading to an increased risk of cap rupture.[7] μOCT showed cholesterol crystals in exquisite detail as linear, highly reflecting structures within a necrotic core (Fig. 3d). Frequently the top and bottom surfaces of the crystals could be identified, representing reflectance from the interfaces between the crystals and the surrounding lipid (Fig. 3d). In one specimen, μOCT was able to resolve a small crystal penetrating through the cap (Fig. 3e).

Microcalcifications and superficial calcium

Microcalcifications have also recently been proposed as a mechanism for compromised cap mechanical integrity.[25] μOCT images of microcalcifications showed accumulations of small, punctate high signal densities within caps and cores of fibroatheroma (Supplementary Fig. 3a). In addition to cap rupture, superficial calcium nodules have also been implicated as a substrate for acute coronary thrombosis and subsequent AMI.[24] In one of our study's specimens, μOCT images showed a calcium plate that was focally exposed to the lumen (Supplementary Fig. 3c). Fine linear structures that likely represent fibrin strands were seen adjoining the exposed calcium to the adjacent intima (Supplementary Fig. 3d), a finding that was confirmed by corresponding histology (Supplementary Fig. 3e).

Bare metal stents (BMS) and drug eluting stents (DES)

Imaging stent microstructure and the surrounding tissue is critical for understanding the response of the artery wall to these implants and for assessing whether or not a stent has adequately healed in order to guide anti-clotting pharmacologic management. By conducting μOCT imaging of undeployed stents, we were able to visualize the polymer coating on drug eluting stents, which appeared as clear rims of material around the metallic struts (Supplementary Fig. 4a). We also found, that at least for one DES type, the μOCT intensity of the polymer was higher when drug was present (Supplementary Fig. 4b). μOCT images of coronary plaques with BMS (Fig. 4a) and DES (Fig. 4b) showed the capability of this technology to visualize the presence and absence of polymer coating *in situ*, respectively.

DES pathology

We found that μOCT allowed the observation of significant heterogeneity in polymer thickness in many DES (Figs. 4c–f). In addition μOCT provided images of a diverse array of DES-related pathology including lifting of the polymer off of the metal strut (Figs. 4c, d), abnormal appearing adhesion of cells over areas of polymer defects (Fig. 4d), apparent cellular infiltrates around the polymer (Fig. 4e), and exposure of the polymer to the luminal surface, without any visible overlying endothelium (Fig. 4f).

DISCUSSION

These results establish that μOCT is capable of visualizing many key cellular and subcellular features relevant to atherogenesis, plaque rupture, thrombosis, and neointimal healing after stenting *in situ*. Because μOCT data is available in three-dimensions and is acquired from intact specimens in their fresh and native states, this technology affords many of the capabilities of three-dimensional histology and SEM in one modality, but with the fidelity, speed, and convenience of imaging *in vivo*. Based on these advantages of the μOCT technology, we believe that it has the potential to make a significant impact in the field of cardiovascular pathology and bench research.

Future development of μOCT for imaging *in vivo* is ongoing[14–18] and new approaches for μOCT catheters are beginning to emerge.[17] When implemented in a coronary catheter, μOCT could open up new opportunities for studying coronary atherosclerosis at the cellular and subcellular level in human patients. One important diagnostic area that could be improved by intracoronary μOCT is the identification and characterization of "vulnerable plaques" or coronary lesions that potentially precipitate thrombosis and AMI. A higher-resolution imaging modality, such as μOCT, that can observe cellular and subcellular features in patients' coronary arteries could allow us to redefine and expand the definition of vulnerable plaque beyond the correlation of related observations to a clinical, cellular, and analytical definition with implications for CAD therapy and prevention of AMI. Intracoronary μOCT could also be a useful tool for monitoring patients who have undergone percutaneous coronary intervention (PCI) and stent implantation. A technique such as this, with sufficient resolution to assess DES strut fibrin or endothelial coverage *in vivo*, may also allow cardiologists to optimize dual antiplatelet therapy duration decisions on an individual

patient basis. The ability of μOCT to visualize polymers could also be utilized to follow dissolution and healing of newer biodegradable stents or scaffolds.[26]

METHODS

μOCT systemand probe optics

OCT measures the electric field amplitude of light that is elastically scattered from within tissue in three dimensions. [8] Depth or axial (z) ranging is achieved by intereferometric measurement of the optical delay of light returned from the sample. μOCT as implemented in this manuscript is based on a form of OCT known as Spectral-domain OCT (SD-OCT). [20] SD-OCT involves parallel detection of spectral interference between light scattered at all depths and a reference, followed by Fourier analysis to obtain a depth-resolved scattering profile. The μOCT system and probe used in this paper differs from conventional OCT devices by employing a very broad bandwidth light source (800±150 nm laser-generated supercontinuum) and a common path reference arm to achieve 1-μm depth or axial (z) resolution. In order to achieve high transverse (x, y) resolutions, we used a relatively high numerical-aperture objective lens (*numerical aperture = 0.12*) to focus the beam onto the sample. We further engineered the focus of the probe beam with an annular apodizer, which reduced the focal spot size from 2.4 to 2.0 μm. Apodization and chromatic dispersion extended the focal depth to ~200 μm, enabling cross-sectional imaging at these high resolutions.

Visualization techniques

For selected images, two-dimensional sections were resliced from three-dimensional μOCT datasets using ImageJ.[27] Volume renderings were computed and displayed using Osirix 3.6.

Human tissue specimens

We examined 80 arterial specimens (20 aorta and 60 coronary) from grossly diseased arterial segments. We obtained fresh aortic segments from National Development and Research Institute, Inc., harvested from patients with known cardiovascular disease and shipped in phosphate buffered saline (PBS) solution on ice within 24 hr post mortem. Coronary arteries were obtained from fresh explanted human hearts (*n = 6*: five male and one female with a mean age of 63.7±7.0) provided by Capital Bioscience, Inc. Explanted hearts were harvested from organ donors following cessation of vital signs, perfused with UW transplant solution and shipped on ice within 24 hrs post mortem. All patients had at least one coronary stent implanted between 2 weeks and 5 years post mortem. We prosected the major coronary arteries from the heart and opened them longitudinally. We identified regions of interest by gross visual inspection and conventional OFDI imaging. Prior to μOCT imaging, we immersed the specimens in PBS at 25 °C and covered them with a thin layer of PBS. We acquired μOCT images from the luminal surface. After imaging, we placed two small ink dots at the beginning of the scan volume to define the initial scan plane. The time between death and μOCT imaging did not exceed 48 hrs. After imaging, we photographed the specimens, fixed them in 10% neutral buffered formalin (Fisher Scientific), decalcified (Cal-Ex, Fisher Scientific), and processed them for routine paraffin-embedded histology. Starting at the registration plane, we captured 5 μm thick histology

sections while sectioning through the tissue block. We stained the sections with Hematoxylin and Eosin. The Institutional Review Board at the Massachusetts General Hospital (IRB #2004P000578) approved the studies using human arterial tissues.

Swine coronary arteries

We acquired endothelium images from fixed swine coronary arteries. We prosected the heart from a sacrificed swine immediately following cessation of vital signs. We flushed the coronary arteries with 100 ml of PBS to remove blood, followed by pressure fixation with a 4% paraformaldehyde solution (US Biochemicals) at a pressure of 100 mm Hg for 30 minutes. We then prosected the fixed coronary segments from the heart, immersed them in a PBS solution at 37 °C, and imaged them with the luminal surface up. The Subcommittee for Animal Research Care at the Massachusetts General Hospital (IACUC 2007N000041) approved the use of discarded swine tissue for these studies.

Endothelial cell culture

Passage 8 Bovine Aortic Endothelial Cells (BAECs), obtained as a gift from Schepens Eye Research Institute and incubated in Dulbecco's Modified Eagle Medium containing 10% fetal bovine serum, 1% L-Glutamine and 1% penicillin-streptomycin, were plated on Nunc® Cell culture coverslips coated with type 1 bovine collagen (50 mg/ml; BD Biosciences). After a confluent monolayer was achieved, we fixed the cells with 2% formalin (Sigma-Aldrich) prior to imaging.

Interpretation of the μOCT images

Using the fiducial ink marks as reference points, we attempted to match the μOCT data with corresponding histopathology images. Due to the subcellular resolution of μOCT, artifacts that occur during histologic processing, and the relatively imprecise nature of histopathology itself, it was difficult to obtain one-to-one cellular-level correlations between all of our images and corresponding microscopic slides. As a result, some μOCT observations are interpretations made by the senior author (G.J.T) who is a pathologist with expertise in coronary pathology.

Supplementary Material

Refer to Web version on PubMed Central for supplementary material.

Acknowledgments

References

1. Virmani R, Kolodgie FD, Burke AP, Farb A, Schwartz SM. Lessons from sudden coronary death - A comprehensive morphological classification scheme for atherosclerotic lesions. Arteriosclerosis Thrombosis and Vascular Biology. 2000; 20:1262–1275.

2. Stary HC, et al. A Definition of Advanced Types of Atherosclerotic Lesions and a Histological Classification of Atherosclerosis: A Report From the Committee on Vascular Lesions of the Council on Arteriosclerosis, American Heart Association. Circulation. 1995; 92:1355–1374. [PubMed: 7648691]

3. Gronholdt MLM, Dalager-Pedersen S, Falk E. Coronary atherosclerosis: determinants of plaque rupture. European Heart Journal. 1998; 19:C24–C29. [PubMed 9597422]

4. Davies MJ. Acute coronary thrombosis - The role of plaque disruption and its initiation and prevention. European Heart Journal. 1995; 16:3–7. [PubMed: 8869011]

5. Pasternak RC, Baughman KL, Fallon JT, Block PC. Scanning electron microscopy after coronary transluminal angioplasty of normal canine coronary arteries. American Journal of Cardiology. 1980; 45

6. Bourassa MG, Cantin M, Sandborn EB, Pederson E. Scanning electron microscopy of surface irregularities and thrombogenesis of polyurethane and polyethylene coronary catheters. Circulation. 1976; 53:992–996. [PubMed: 1269137]

7. Abela GS, Aziz K. Cholesterol crystals rupture biological membranes and human plaques during acute cardiovascular events--a novel insight into plaque rupture by scanning electron microscopy. Scanning. 2006; 28:1–10. [PubMed: 16502619]

8. Huang D, et al. Optical coherence tomography. Science. 1991; 254:1178–1181. [PubMed: 1957169]

9. Jang IK, et al. Visualization of coronary atherosclerotic plaques in patients using optical coherence tomography: Comparison with intravascular ultrasound. J Am Coll Cardiol. 2002; 39:604–609. [PubMed: 11849858]

10. Yun SH, et al. Comprehensive volumetric optical microscopy in vivo. Nature Medicine. 2006; 12:1429–1433.

11. Tearney GJ, et al. Three-Dimensional Coronary Artery Microscopy by Intracoronary Optical Frequency Domain Imaging. Journal of the American College of Cardiology: Cardiovascular Imaging. 2008; 1:752–761. [PubMed: 19356512]

12. Boppart SA, et al. In vivo cellular optical coherence tomography imaging. Nature Medicine. 1998; 4:861–865.

13. Povazay B, et al. Submicrometer axial resolution optical coherence tomography. Opt Lett. 2002; 27:1800–1802. [PubMed: 18033368]

14. Ralston TS, Marks DL, Carney PS, Boppart SA. Interferometric synthetic aperture microscopy. Nat Phys. 2007; 3:129–134. [PubMed: 25635181]

15. Liu LB, Liu C, Howe WC, Sheppard CJR, Chen NQ. Binary-phase spatial filter for real-time swept-source optical coherence microscopy. Opt Lett. 2007; 32:2375–2377. [PubMed: 17700790]

16. Ding ZH, Ren HW, Zhao YH, Nelson JS, Chen ZP. High-resolution optical coherence tomography over a large depth range with an axicon lens. Opt Lett. 2002; 27:243–245. [PubMed: 18007767]

17. Lee KS, Rolland LP. Bessel beam spectral-domain high-resolution optical coherence tomography with micro-optic axicon providing extended focusing range. Opt Lett. 2008; 33:1696–1698. [PubMed: 18670507]

18. Leitgeb RA, Villiger M, Bachmann AH, Steinmann L, Lasser T. Extended focus depth for Fourier domain optical coherence microscopy. Opt Lett. 2006; 31:2450–2452. [PubMed: 16880852]

19. Vakhtin AB, Kane DJ, Wood WR, Peterson KA. Common-path interferometer for frequency-domain optical coherence tomography. Appl Opt. 2003; 42:6953–6958. [PubMed: 14661810]

20. Hausler G, Lindner MW. "Coherence Radar" and "Spectral Radar"---New Tools for Dermatological Diagnosis. Journal of Biomedical Optics. 1998; 3:21–31. [PubMed: 23015002]

21. Finn AV, et al. Pathological correlates of late drug-eluting stent thrombosis -Strut coverage as a marker of endothelialization. Circulation. 2007; 115:2435–2441. [PubMed: 17438147]

22. Libby P. Changing concepts of atherogenesis. Journal of Internal Medicine. 2000; 247:349–358. [PubMed: 10762452]

23. Lusis AJ. Atherosclerosis. Nature. 2000; 407:233–241. [PubMed: 11001066]

24. Virmani R, Burke AP, Farb A, Kolodgie FD. Pathology of the vulnerable plaque. J Am Coll Cardiol. 2006; 47:C13–C18. [PubMed: 16631505]

25. Vengrenyuk Y, Cardoso L, Weinbaum S. Micro-CT based analysis of a new paradigm for vulnerable plaque rupture: cellular microcalcifications in fibrous caps. Molecular & Cellular Biomechanics. 2008; 5

26. Serruys PW, et al. A bioabsorbable everolimus-eluting coronary stent system (ABSORB): 2-year outcomes and results from multiple imaging methods. Lancet. 2009; 373:897–910. [PubMed: 19286089]

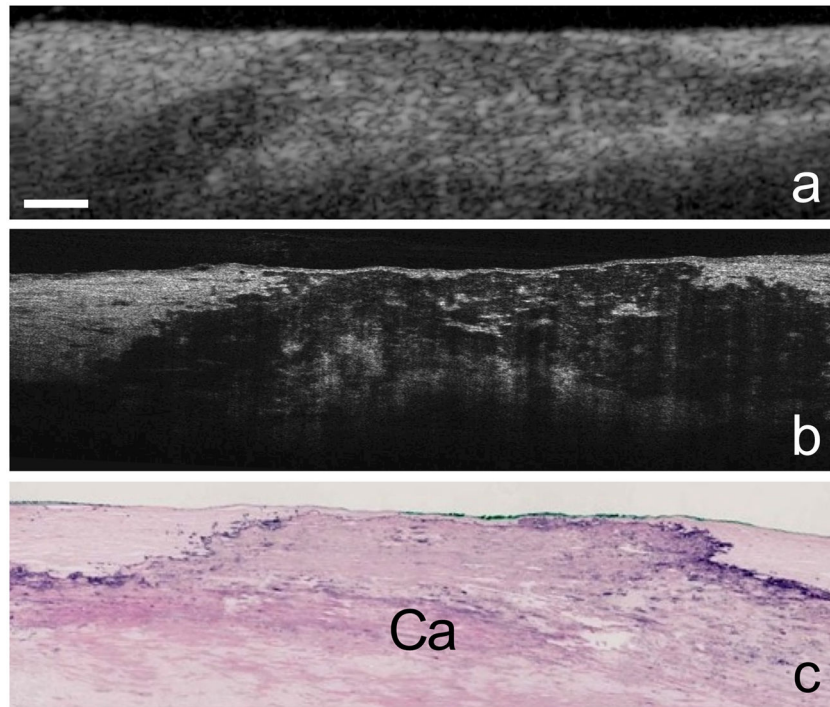27. Rasband, WS. Health, NIo. ImageJ. Bethesda, MD: 1997–2009.

Figure 1. μOCT images of a human coronary plaque

Human cadaver specimen. Comparison between corresponding OCT (**a**), μOCT (**b**), and histology images (**c**, Hematoxylin and Eosin) of a calcium plate (Ca) within the coronary artery wall. Scale bar, 200 μm.
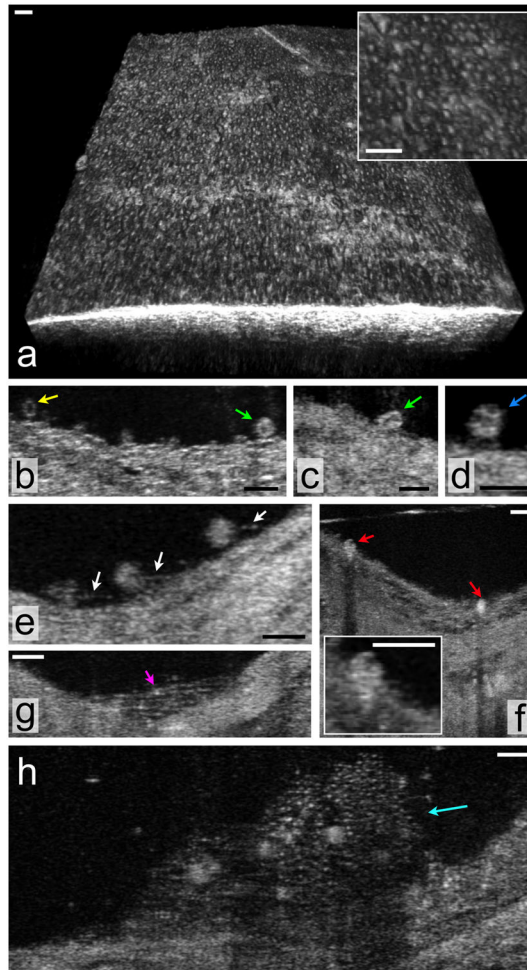
Figure 2. µOCT of superficial arterial morphology
(**a**) Three-dimensional rendering of the swine coronary artery *ex vivo*, demonstrating a pattern of raised cells that are consistent with endothelial "pavementing". (**b**–**h**) Human cadaver specimens. (**b**) Multiple cells that are likely leukocytes (arrows) are seen adhering to the luminal surface in this µOCT image of a coronary plaque. Two different cell morphologies can be observed, one smaller cell with scant cytoplasm, consistent with a lymphocyte (yellow arrow) and another, slightly larger cell with a highly scattering, abundant cytoplasm, suggestive of a monocyte (green arrow). (**c**) Cell with an indented, bean-shaped nucleus (green arrow) characteristic of a monocyte. (**d**) Cell with a multi-lobed nucleus, possibly a neutrophil (blue arrow), is attached to the endothelial surface. (**e**) Multiple leukocytes tethered to the endothelial surface by linear structures suggestive of pseudopodia (white arrows). (**f**) Cells with the morphology of monocytes (red arrows) are seen in this cross-section and inset to be transmigrating through the endothelium. (**g**) Structures consistent with fibrin (magenta arrow) are visible as linear strands bridging a gap in the coronary artery wall. (**h**) Thrombus (cyan arrow) that appears to contain fibrin, small (2–3 µm diameter) highly scattering structures likely to be platelets, and multiple, entrapped cells. Scale bars, 30 µm.
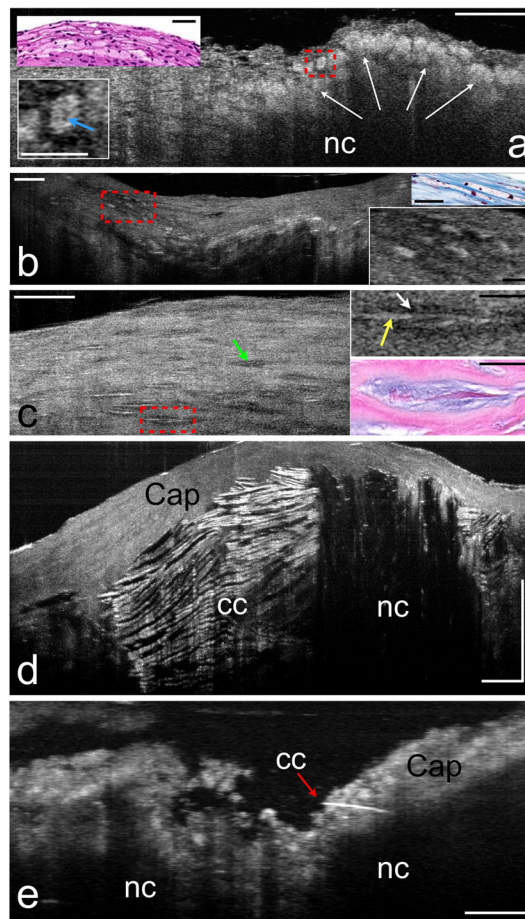
Figure 3. µOCT of plaque morphology

Human cadaver specimens. (**a**) Necrotic core (nc) fibroatheroma with highly scattering lipid-laden macrophages or foam cells (white arrows) infiltrating the cap, also seen in the corresponding histology (upper left inset). An intracellular region of low µOCT signal, which may represent the nucleus, can be observed within the cytoplasm of some foam cells (e.g. lower left inset, blue arrow). (**b**) Another lesion, visualized by µOCT and histology, contains highly scattering foam cells that are ellipsoidal (right insets). (**c**) Smooth muscle cells by µOCT appear as spindle-shaped cells (green arrow). Smooth muscle cells producing collagen have a high backscattering interior (right upper inset, yellow arrow) and a "halo" of low backscattering (right upper inset, white arrow). Matching histology (right lower inset) demonstrates that the high backscattering region represents the cell body, while the lower intensity halo corresponds to collagen matrix. (**d**) Large necrotic core (nc) fibroatheroma, demonstrating cholesterol crystals (cc), characterized by reflections from their top and bottom surfaces. (**e**) A thin crystal (red arrow) appears to be piercing the cap of another necrotic core (nc) plaque. Scale bars for all primary images, 100 µm. Scale bars for all insets, 30 µm.
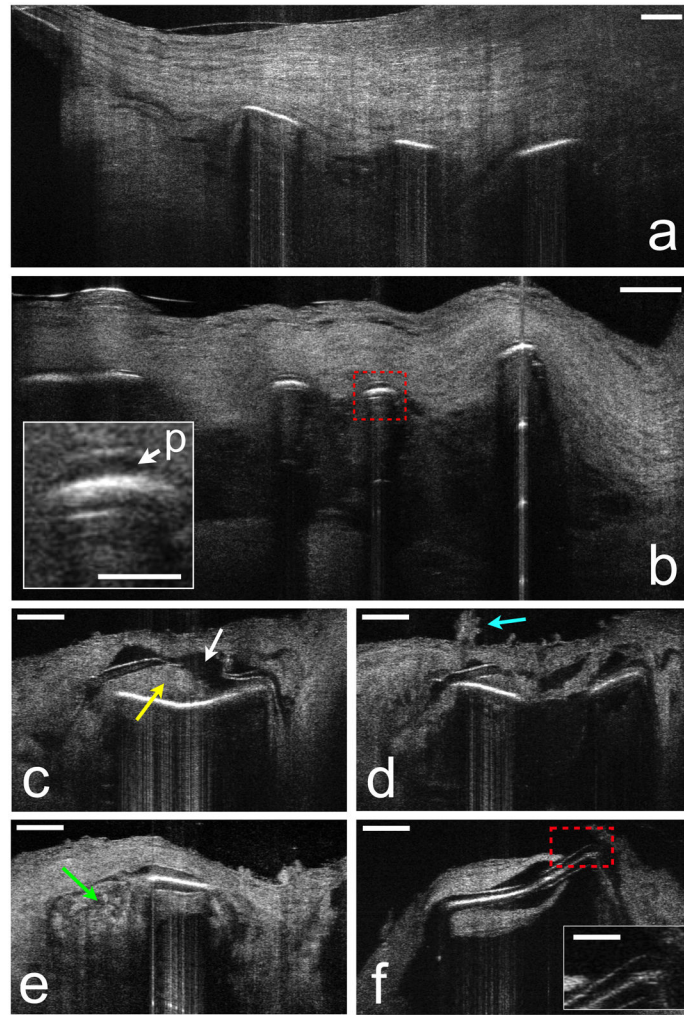
Figure 4. μOCT of stent and neointimal morphology

Human cadaver specimens. (a) μOCT image from a coronary segment with an implanted BMS shows struts devoid of polymer, covered by neointima. (**b**) DES struts from another cadaver showing polymer (red dashed box and p, inset) overlying the strut reflections. (**c**) Tissue (yellow arrow) is interposed between the polymer and the stent strut and the polymer has fractured (white arrow). (**d**) Superficial leukocyte cluster (cyan arrow) and adjacent attached leukocytes overlying the site of the polymer fracture. (**e**) Apparent inflammation at the edge of a strut (green arrow). (**f**) Uncovered strut, completely devoid of overlying endothelium (red dashed box and inset). Scale bars for primary images, 100 μm. Scale bars for all insets, 30 μm.